

# Two dimensional grating magneto-optical trap

Eric Imhof\* and Benjamin Stuhl  
*Space Dynamics Laboratory, Logan, Utah 84341, USA*

Brian Kasch, Bethany Kroese, Spencer Olson, and Matthew B. Squires  
*Air Force Research Laboratory, Kirtland AFB, New Mexico 87117, USA*  
(ΩDated: December 14, 2024)

We demonstrate a two dimensional grating magneto-optical trap (2D GMOT) with a single input beam and a planar diffraction grating in  $^{87}\text{Rb}$ . This configuration increases experimental access when compared with a traditional 2D MOT. As configured in the paper, the output flux is several hundred million rubidium atoms/s at a mean velocity of  $19.0 \pm 0.2$  m/s. The velocity distribution has a  $3.3 \pm 1.7$  m/s standard deviation. We use the atomic beam from the 2D GMOT to demonstrate loading of a three dimensional grating MOT (3D GMOT) with  $2.02 \times 10^8 \pm 3 \times 10^6$  atoms. Methods to improve flux output are discussed.

PACS numbers: 37.10.De, 37.10.Gh, 07.77.Gx, 37.20.+j

Keywords: grating MOT, magneto-optical trap, cold atom source

## I. INTRODUCTION

Matter wave interferometry has demonstrated multiple order of magnitude improvements over a wide range of precision measurements [1–8]. These successes have spurred interest in transitioning cold atom devices from the lab to more demanding environments [9–17]. Recently, a three dimensional grating magneto-optical trap (3D GMOT) was demonstrated that satisfies many needs of a deployable system [18–20]. As shown in Fig. 1(a), a 3D GMOT is formed when a single laser beam is normally incident on a set of planar diffraction gratings. The diffracted beams intersect with the incident light. Atoms are captured within the region of beam overlap, assuming proper conditions of polarization and detuning. The 3D GMOT shows comparable atom number scaling to standard six-beam MOT's [18] and is able to achieve sub-Doppler cooling [21].

A similar principle can be used to form a two dimensional GMOT (2D GMOT), Fig. 1(b), resulting in a cold atomic beam. Adapting from the 3D to the 2D case requires different design considerations which will be detailed here.

The 2D GMOT is used to load a 3D GMOT at a different location. By separating the source vapor from the experimental region, the 2D GMOT enables faster loading rates and higher atom number in the 3D GMOT without significantly adding to the size, weight, power, and cost of the overall system.

Both the 2D and 3D GMOT share promising features. First, the total laser power required is reduced compared to other competitive MOT schemes. Second, the atoms are captured above a planar surface, reducing obstruction. Third, most of the MOT requirements, such as alignment, polarization, and intensity balance, are deter-

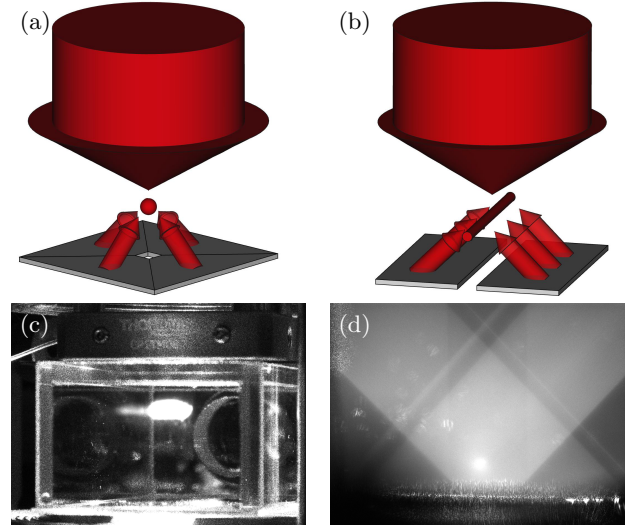


FIG. 1. (Color online) A laser beam impinges on a series of diffraction gratings to form (a) a 3D GMOT or (b) a 2D GMOT. Images (c) and (d) show fluorescence of the 3D GMOT and 2D GMOT viewed along its axis.

mined by the grating design, alleviating concerns about reproducibility.

In this paper, we show the design and characteristics of a 2D GMOT with Doppler cooling along the atom beam axis (the  $2\text{D}^+$  configuration) [22]. We use the  $2\text{D}^+$  GMOT to load a 3D GMOT, and report the loading rates, lifetime, and atom number of the combined system.

## II. THEORY AND DESIGN

To properly choose gratings and laser parameters such as intensity and polarization, it is necessary to understand the forces at work in a GMOT. Each atom in

\* eric.imhof@sdl.usu.edu

a MOT scatters light from multiple off-resonant laser beams with wavevectors  $\mathbf{k}_j$  and polarization vectors  $\hat{\epsilon}_j$ . Assuming the atom absorbs from  $F = 0 \rightarrow F' = 1$ , a circularly polarized beam drives transitions to the  $m_F = -1, 0, +1$  excited states with relative strengths  $\alpha_{m_F}(\varphi, \hat{\epsilon}_j)$  that depend on the angle between the wavevector and the local magnetic field  $\varphi$ . The average force from a single beam  $j$ , of intensity  $I_j$ , on an atom with velocity  $\mathbf{v}$  in a magnetic field  $\mathbf{B}$  is

$$\mathbf{F}_j = \hbar \mathbf{k}_j \frac{\Gamma}{2} \frac{I_j}{I_{sat}} \sum_{m_F=-1,0,1} \frac{\alpha_{m_F}(\varphi, \hat{\epsilon}_j)}{1 + \frac{\sum_j I_j}{I_{sat}} + \frac{4(\Delta - \mathbf{k}_j \cdot \mathbf{v} - \mu_F m_F B/\hbar)^2}{\Gamma^2}}, \quad (1)$$

where  $\Gamma$  is the natural linewidth and  $\Delta = \omega_L - \omega_0$ , the detuning of the laser frequency from the transition.  $I_{sat}$  is the saturation intensity and  $\mu_F = g_F \mu_B$ . The transition strengths are  $\alpha_{\pm 1} = (1 \mp s \cos \varphi)^2/4$  and  $\alpha_0 = (\sin^2 \varphi)/2$ , where  $s = \pm 1$  denotes left or right circular beam polarization, respectively. In the limit of small Doppler and Zeeman shifts, the force becomes

$$\mathbf{F}_j \approx \hbar \mathbf{k}_j \frac{\Gamma}{2} \frac{I_j}{I_{sat}} \left[ K + C \left( \mathbf{k}_j \cdot \mathbf{v} - \frac{\mu_F s}{\hbar} \frac{\mathbf{k}_j \cdot \mathbf{B}}{|\mathbf{k}_j|} \right) \right], \quad (2)$$

where  $K = (1 + \sum_j I_j/I_{sat} + 4\Delta^2/\Gamma^2)^{-1}$ ,  $C = 8\Delta K^2/\Gamma^2$  [23].

For most MOT configurations, lasers approach the trap along the principal axes of the magnetic field. Accordingly,  $|\mathbf{k}_j \cdot \mathbf{B}| = 1$ , so trapping is optimized for pure circular polarization. In a GMOT, the wavevector of each diffracted beam is not aligned with the magnetic field. Therefore, the optimal light field does not have pure circular polarization. Gratings are selected which balance the necessary contributions of each transition to form a trap. These requirements differ between the 2D and 3D GMOT, as shown in the following.

A circularly polarized beam with intensity  $I_1$ , normally incident on gratings, will diffract upwards at an angle  $\theta$  from normal ( $+\hat{\mathbf{y}}$ ) with intensity  $I_{up}$ , as shown in Fig. 2. The incident beam has  $\mathbf{k}_1 = -|k|\hat{\mathbf{y}}$  and  $s = +1$ , denoting pure circular polarization. If the magnetic field, centered on the beam overlap region, is  $\mathbf{B} = G(x\hat{\mathbf{x}} - y\hat{\mathbf{y}})$ , the force from beam 1 is

$$\mathbf{F}_1 \approx -\hbar k \frac{\Gamma}{2\pi} \frac{I_1}{I_{sat}} \left[ K + C \left( -kv_y - \frac{\mu_F G}{\hbar} y \right) \right] \hat{\mathbf{y}}. \quad (3)$$

In general, gratings do not preserve polarization. The diffracted beams will have a fractional intensity  $P_+ I_{up}$  in the  $s = +1$  polarization and  $P_- I_{up}$  in the  $s = -1$  polarization. Summing over the polarizations, the total force in  $\hat{\mathbf{x}}$  is

$$\mathbf{F}_x \approx \hbar k C \Gamma \sin^2 \theta \frac{I_{up}}{I_{sat}} \left( kv_x + (P_- - P_+) \frac{\mu_F G}{\hbar} x \right) \hat{\mathbf{x}}. \quad (4)$$

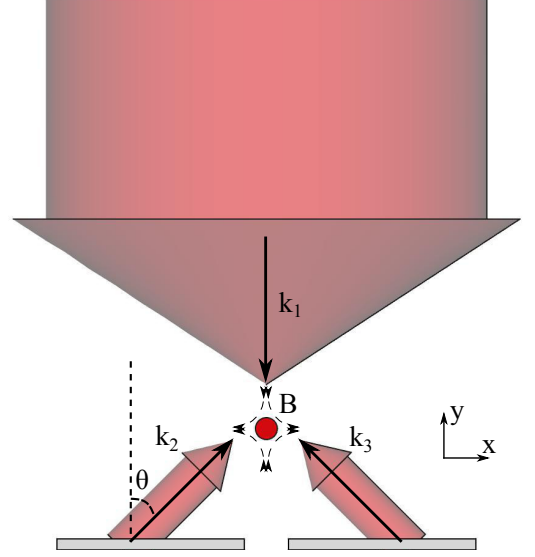


FIG. 2. (Color online) The  $\mathbf{k}$  vectors and  $\mathbf{B}$  field to model a 2D GMOT.

Similarly,

$$\begin{aligned} \mathbf{F}_y \approx & \hbar k \Gamma K \cos \theta \frac{I_{up}}{I_{sat}} \\ & + \hbar k \Gamma C \cos \theta \frac{I_{up}}{I_{sat}} \left( kv_y \cos \theta + 2(P_+ - P_-) \frac{\mu_F G}{\hbar} y \cos \theta \right) \\ & - \hbar k \frac{\Gamma}{2} \frac{I_1}{I_{sat}} \left[ K + C \left( -kv_y - \frac{\mu_F G}{\hbar} y \right) \right] \hat{\mathbf{y}}. \end{aligned} \quad (5)$$

The constant terms (i.e. those  $\propto K$ ) represent an intensity mismatch that will shift the trap center if not properly balanced. In particular, a trap will only form at the field zero if

$$I_{up} = \frac{I_1}{2 \cos \theta}. \quad (6)$$

Then,

$$\mathbf{F}_x \approx \hbar k C \frac{\Gamma}{2} \frac{I_1}{I_{sat}} \frac{\sin^2 \theta}{\cos \theta} \left( kv_x + (P_- - P_+) \frac{\mu_F G}{\hbar} x \right) \hat{\mathbf{x}}, \quad (7)$$

$$\begin{aligned} \mathbf{F}_y \approx & \hbar k C \frac{\Gamma}{2} \frac{I_1}{I_{sat}} \left( kv_y (1 + \cos \theta) \right. \\ & \left. + \frac{\mu_F G}{\hbar} y (1 + (P_+ - P_-) \cos \theta) \right) \hat{\mathbf{y}}. \end{aligned} \quad (8)$$

Note that because  $\Delta$  is negative, these forces perform trapping and cooling.

Eq. (6) shows the ideal intensity balance between the three beams of the 2D GMOT. However, a subtle distinction separates Eq. (6) from the necessary grating efficiency. Gratings compress the diffracted beam area with respect to the originally incident light. Thus, a perfectly efficient grating (i.e. 100% of input power directed into the first order) would produce  $I_{up} = I_1 / \cos \theta$ . As a result, satisfying Eq. (6) requires a grating efficiency of 50%, independent of  $\theta$ . If not, the resulting intensity imbalance manifests as an offset in the trap location from the field zero along the axis normal to the gratings [24]. In general, for a GMOT with  $N$  diffracted beams, the ideal grating efficiency is  $1/N$ .

The relatively high ( $1/N = 50\%$ ) efficiency requirements of the 2D GMOT preclude many grating types. Any grating without a preferred direction (i.e. blazed gratings) would have to diffract practically all power into the  $\pm$  first orders.

Custom non-directional etched gratings have been fabricated to this standard for the 3D GMOT [18] [25] [26], albeit with a high input of design time and fabrication cost. Such gratings often require e-beam lithography for small ( $\approx 500$  nm) feature sizes. Manufacturing large area gratings requires significant time in high-demand clean room facilities, motivating our experiment to investigate the option of using replicated blazed gratings.

Replicated gratings are inexpensive and readily available, but confined to existing master gratings. Additionally, replicated gratings are not designed to minimize residual specular reflections, which can undermine trap performance by driving anti-trapping transitions in the atoms. To avoid reflected light, GMOT systems with blazed gratings have gaps between gratings aligned with the central axis of the input laser.

In addition to intensity balance, the polarization of the diffracted beams significantly effects the force equations. In particular, maximizing trapping in the  $x$  direction requires  $P_- = 1$  and  $P_+ = 0$ , as shown in Fig. 3(a). However, this polarization minimizes trapping in the  $y$  direction.

Fig. 3 shows the effect of imperfect polarization on the trapping forces by adjusting the ratio of  $P_+$  to  $P_-$  within the 50% diffraction efficiency constraint. Fig. 3(a)-(d) show  $(P_+, P_-) = (0, 1), (0.1, 0.9), (0.2, 0.8)$ , and  $(0.3, 0.7)$ , respectively. The linear approximation of  $\mathbf{F}_x$  from Eq. (7) is shown as a dashed line. The force along  $y$  increases at the expense of the  $x$  trapping strength. Equal trapping strength along each axis can be achieved for  $P_- - P_+ = \cos \theta$ . For the case of  $\theta = 45^\circ$ , equal trapping is achieved for  $P_- \approx 0.85$  and  $P_+ \approx 0.15$ .

Fig. 4 shows the theoretical diffraction efficiencies of two commercially produced ruled gratings with different groove spacings and blaze angles for the case of normal incidence. The efficiencies depend on both wavelength and incident polarization. The results for the polarization parallel and perpendicular to the groove direction combine to give the average efficiency, shown as the thick blue curve.

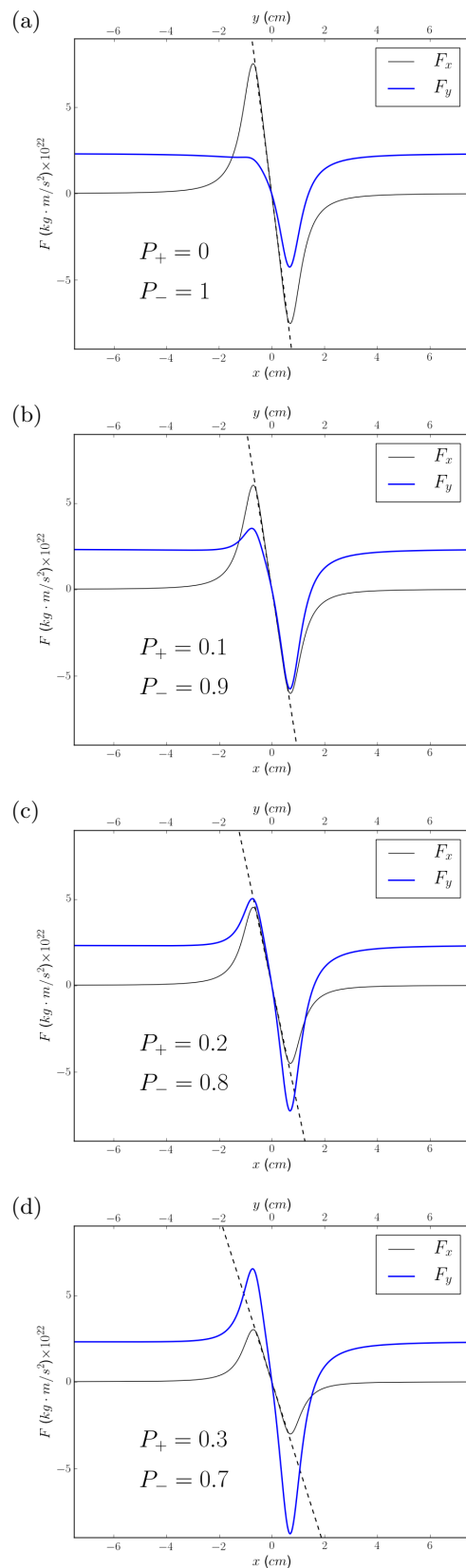


FIG. 3. (Color online) Trapping forces in a 2D GMOT for varying polarizations of the diffracted beams, assuming 50% total efficiency. Thin black curves show  $\mathbf{F}_x$  and thick blue curves show  $\mathbf{F}_y$ . Dashed black lines are the linear approximation of  $\mathbf{F}_x$  from Eq. (7). Plots (a)-(d) show  $(P_+, P_-) = (0, 1), (0.1, 0.9), (0.2, 0.8)$ , and  $(0.3, 0.7)$ , respectively.

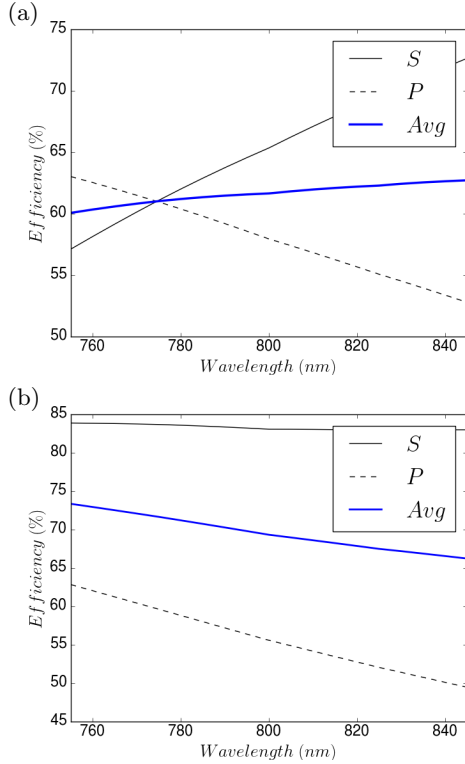


FIG. 4. (Color online) Grating efficiencies as a function of wavelength at normal incidence for two gratings of interest in magneto-optical trapping. Figure (a) shows efficiencies for grating  $G1$  with 900 grooves/mm and an 1000 nm blaze wavelength, while (b) shows grating  $G2$  with 830 g/mm and an 800 nm blaze.

We operate with  $^{87}\text{Rb}$ , cooled on the  $5^2S_{1/2} \rightarrow 5^2P_{3/2}$ ,  $F = 2 \rightarrow 3$  transition at  $\lambda = 780.246$  nm. A grating  $G1$  (Fig. 4(a)) with 900 grooves/mm and 1000 nm blaze wavelength provides equal linear polarization efficiencies near 60%. Equal linear polarization should result in a circularly polarized diffracted beam.

However, as discussed above, a pure circular polarization does not provide equal trapping strength along each axis. A different grating  $G2$  (Fig. 4(b)) with 830 grooves/mm and an 800 nm blaze diffracts a small fraction of its power into the opposing circular handedness, aiding trapping along the  $x$  direction. We measure the overall diffraction efficiency of  $G2$  at 68% with  $P_+ = 0.061$  and  $P_- = 0.939$ .

Because the gratings are located outside of the vacuum cell, the optical surfaces of the glass chamber modify the intensity and polarization of the diffracted beams. As a result, the overall efficiency of  $G2$  drops to 64%, with  $P_+ = 0.066$  and  $P_- = 0.934$ . Both gratings  $G1$  and  $G2$  were tested but only  $G2$  produces a 2D GMOT.

While  $G1$  is unsuccessful in this experiment, it should be noted that the input light has a Gaussian intensity profile. As a result, the diffracted intensity is further diminished compared to the peak input intensity along the central axis. If the input light had a more uniform

profile, we expect  $G1$  to create a trap. Similarly, it is possible that  $G2$  diffracts too strongly for a uniform intensity profile.

For the 2D GMOT, two  $17.5 \times 38$  mm<sup>2</sup> rectangular gratings are placed with their blazes facing towards the central axis, separated by a 5 mm gap. For the 3D GMOT, four trapezoidal gratings are combined to produce a  $38 \times 38$  mm<sup>2</sup> square with a  $4 \times 4$  mm<sup>2</sup> gap at its center, as shown in Fig. 5. Again, all the blazes point towards the central axis. However, because the 3D gratings produce  $N = 4$  diffracted beams, the 3D GMOT requires an efficiency closer to 25%. To reduce the diffracted beam power, a 0.1 ND filter is placed between the 3D gratings and the vacuum chamber wall.

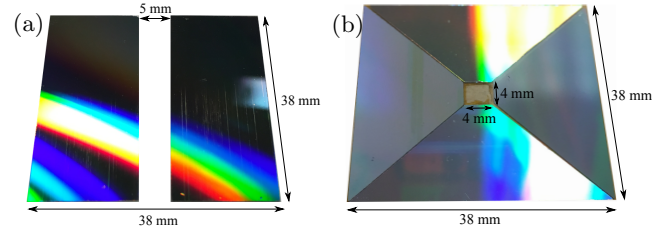


FIG. 5. (Color online) The gratings used for the (a) 2D GMOT and (b) 3D GMOT.

### III. EXPERIMENTAL SETUP

The experiment uses two epoxied glass vacuum cells [27] separated by a mini-conflat flange cross, as shown in Fig. 6. All glass walls are anti-reflection coated on both sides for 780 nm. The system pressure was  $2 \times 10^{-9}$  Torr as measured by a residual gas analyzer on a pumping station a few meters from the experimental chambers. The 2D GMOT is produced in a chamber  $30 \times 40 \times 72$  mm<sup>3</sup>, which is capped by a silicon reflector with a 1 mm diameter pinhole. The atom beam travels through the pinhole, then through a second filtering 3 mm pinhole in the copper gasket of the conflat cross. The atoms are then collected on the opposing side of the cross in a 3D GMOT in a  $25 \times 40 \times 85$  mm<sup>3</sup> chamber.

A single laser beam is input into each chamber with 11.0 mW/cm<sup>2</sup> light red detuned from the cycling transition and 3.8 mW/cm<sup>2</sup> at the repump transition for  $^{87}\text{Rb}$ . The light is emitted from a single mode, polarization-maintaining fiber and expanded through a negative lens. A wide-angle quarter wave plate provides circular polarization to the expanding beam, which is then reflected from a two inch mirror and collimated with a 100 mm focal length lens.

A “push” beam is directed along the 2D GMOT axis to provide enhanced cooling, using 3.3 mW of cooling light in a beam with a 4 mm waist. The beam is retro-reflected from the polished silicon reflector with the 1 mm exit pinhole. We refer to the enhanced beam as a 2D<sup>+</sup> GMOT

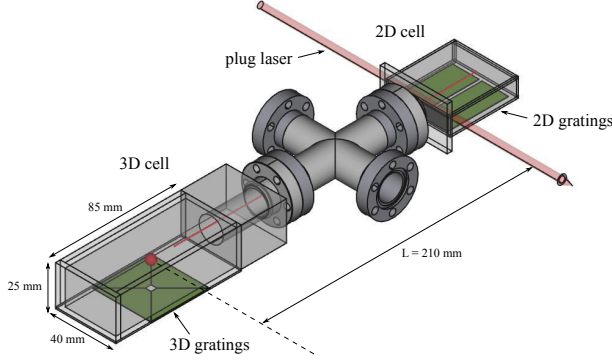


FIG. 6. (Color online) The experimental setup for a 2D GMOT loading a 3D GMOT. Input lasers and magnetic field sources are omitted for clarity.

Four permanent neodymium magnets are arranged along the corners of the  $2D^+$  GMOT chamber, creating an extended quadrupole magnetic field with a 20 G/cm gradient. They are positioned via a three axis translation stage and a tip-tilt mirror mount to aid alignment of the  $2D^+$  GMOT with the silicon pinhole. The 3D GMOT magnetic fields are produced by an anti-Helmholtz coil pair, centered by cage rods that align the 3D GMOT optics. At 1.2 A current, they provide an axial gradient of 10 G/cm.

#### IV. DIAGNOSTICS

The 3D GMOT fluorescence is monitored using a photodiode (Thorlabs PDA100A). Light from the GMOT is collected using a  $f = 25.4$  mm lens positioned  $2f$  from the trap and the sensor surface. Switching the 3D GMOT's magnetic field on produces a rising fluorescence signal proportional to the number of captured atoms. The 3D GMOT atom number  $N(t)$  is described with the capture rate  $R_{capture}$  and trap lifetime  $\tau_{trap}$  by

$$N(t) = \tau_{trap} R_{capture} (1 - e^{-t/\tau_{trap}}). \quad (9)$$

The  $2D^+$  GMOT beam can be characterized by monitoring the 3D GMOT fluorescence as a function of time. An 8 mW “plug” laser beam is positioned just after the exit pinhole, as seen in Fig. 6. The plug laser acts to misalign the atomic beam from the 3D GMOT, effectively reducing  $R_{capture}$ . If the plug beam is turned off for a short period, the 3D GMOT will grow as atoms traverse the distance  $L$  from the exit pinhole to the capture volume of the 3D trap, as shown in Fig. 7.

Two models are used to analyze the  $2D^+$  GMOT flux using the transient response of the 3D GMOT. The first model assumes the atoms start at the exit pinhole of the 2D chamber with a singular speed  $v_0$  and that the number of atoms reaching the capture volume per unit

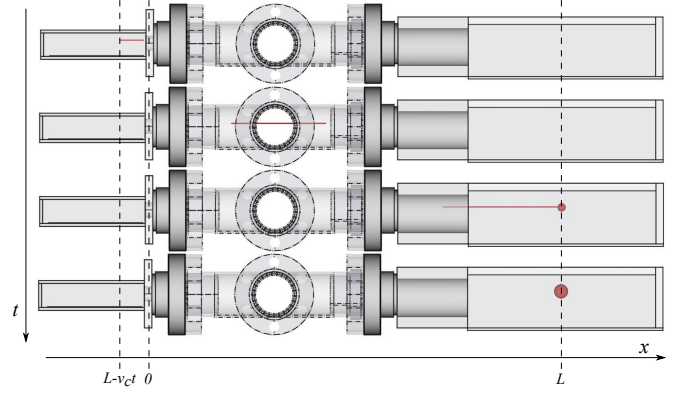


FIG. 7. (Color online) A short pulse of the  $2D^+$  GMOT is released at  $t = 0$ , traverses a distance  $L$ , and is captured in a 3D GMOT, which grows as a function of time.

time is  $R_{capture}$ . The atom number will be zero for times  $0 < t < \Delta T = L/v_0$ , and then grow linearly according to

$$N(t) = R_{capture}(t - \Delta T). \quad (10)$$

In the second model, the  $2D^+$  GMOT before the plug beam is turned off is described as a distribution of atoms in position and velocity

$$\eta(z, v) = \frac{A}{\sigma\sqrt{2\pi}} \exp\left(-\frac{(v - v_0)^2}{2\sigma^2}\right), \quad (11)$$

where  $A$  represents the number of atoms/m in the beam, weighted by a normal distribution in velocity with peak  $v_0$  and spread  $\sigma$ . That is, the density of atoms with velocities between  $v_1$  and  $v_2$  is given by  $A \int_{v_1}^{v_2} \exp[-(v - v_0)^2/2\sigma^2] / \sigma\sqrt{2\pi} dv$ . The normal distribution represents a low temperature approximation of the thermal velocity distribution.

When the plug beam is turned off, the 3D GMOT grows as atoms reach the capture volume in time  $t$  with  $v < v_c$ , the capture velocity of the trap. For  $t \ll \tau_{trap}$ , loss terms can be neglected. Defining the exit pinhole to be at  $z = 0$ ,

$$\begin{aligned} N(t) &= \int_{L-v_c t}^0 \int_{(L-z)/t}^{v_c} \eta(z, v) dv dz \\ &= A \frac{\sigma t}{\sqrt{2\pi}} \left( \exp\left[-\frac{(v_0 - \frac{L}{t})^2}{2\sigma^2}\right] - \exp\left[-\frac{(v_c - v_0)^2}{2\sigma^2}\right] \right) \\ &\quad + \frac{A}{2} (v_0 t - L) \left( \operatorname{erf}\left[\frac{v_0 - \frac{L}{t}}{\sigma\sqrt{2}}\right] + \operatorname{erf}\left[\frac{v_c - v_0}{\sigma\sqrt{2}}\right] \right). \end{aligned} \quad (12)$$

The distribution  $\eta(z, v)$  leads to a more experimentally useful result, the flux  $\Phi(v)dv$ , defined as the number of atoms exiting the pinhole at velocity  $v$  per unit time. The normal approximation for  $\eta$  yields



$$\Phi(v) = v\eta(z, v) = \frac{A}{\sigma\sqrt{2\pi}} v \exp\left(-\frac{(v - v_0)^2}{2\sigma^2}\right). \quad (13)$$

## V. RESULTS

Fig. 8 shows the rise in atom number when the 3D magnetic coils were switched on. The solid curve is a fit to Eq. (9) in which  $R_{capture} = 9.97 \times 10^7 \pm 5 \times 10^5$  atoms/s and  $\tau_{trap} = 2.03 \pm 0.02$  seconds. The steady state MOT number was  $2.02 \times 10^8 \pm 3 \times 10^6$  atoms.

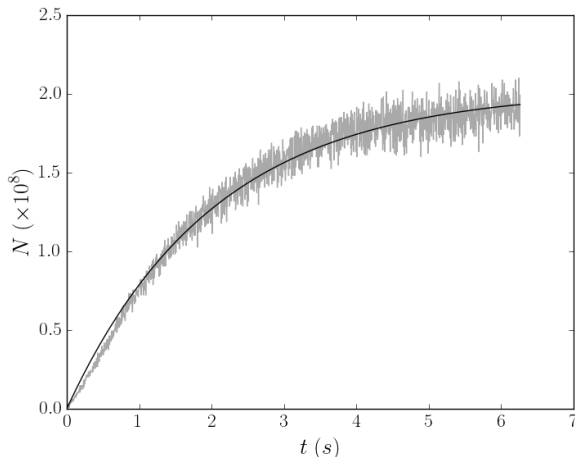


FIG. 8. Atom number vs. time after 3D GMOT magnetic field is switched on.

The plug beam was then applied to reduce  $R_{capture}$ . The plug beam was turned off for 197 ms and the resulting 3D GMOT growth is shown in Fig. 9. The data was collected by an average of 16 independent runs and then smoothed using a centered simple moving average. The dashed line uses Eq. (10) with  $R_{capture} = 7 \times 10^7$  atoms/s and  $\Delta T = 11.0$  ms. The solid curve is a fit using Eq. (12) with  $A = 3.51 \times 10^6 \pm 5 \times 10^4$  atoms/m,  $\sigma = 3.3 \pm 1.7$  m/s, and  $v_0 = 19.0 \pm 0.2$  m/s.

It should be noted that the plug beam used detuned light and did not act as a perfect shutter. Because some flux continued to feed the 3D GMOT, the reported values for  $R_{capture}$  represent the fraction of atomic flux that was affected by the plug beam.

Assuming typical atom beam divergence as discussed in [28], it is likely that only  $\approx 25\%$  of the  $2D^+$  GMOT beam actually entered the capture volume of the 3D GMOT. Using Eq. (13), we therefore estimate the total flux at the pinhole to be  $> 4 \times 10^8$  atoms/s.

## VI. COMPARISONS AND OUTLOOK

Traditional  $2D^+$  MOT's have flux values as high as  $10^{11}$  atoms/s [29]. However, these  $2D^+$  MOT's form

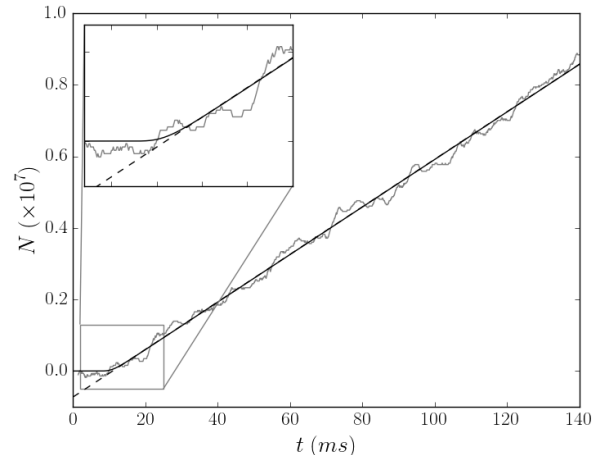


FIG. 9. 3D GMOT atom number vs. time as plug laser beam is turned off, allowing the  $2D^+$  GMOT to load the 3D GMOT. The dashed line assumes no spread in the velocity distribution of the  $2D^+$  GMOT, as in Eq. (10). The solid curve is a fit using Eq. (12), which accounts for a range of velocities.

across 10 cm lengths or higher and saturate with laser intensities near  $20 \text{ mW/cm}^2$ . By comparison, the  $2D^+$  GMOT reported here forms over a length of several mm with  $11 \text{ mW/cm}^2$  laser intensity. The short beam length was expected, as circular Gaussian beams cause the input intensity profile to vary significantly, limiting the range over which optimal cooling parameters are achieved. Future work will employ beam shaping techniques to create a top hat intensity profile within the trap region. A top hat intensity profile will also help make more effective use of available laser power to enable higher intensity beams.

Increasing the  $2D^+$  GMOT length allows atoms with higher longitudinal velocities to be collimated into the MOT beam [29–31]. Assuming the pressure is low enough that collisions are negligible, the flux should scale linearly with increased length. Additionally, increasing the laser intensity acts to raise the transverse capture velocity of a  $2D^+$  MOT, further increasing total flux.

Prior work has shown that the 3D GMOT atom number saturates with input intensities near  $50 \text{ mW/cm}^2$  [18], compared to our  $11 \text{ mW/cm}^2$ . Despite the difference, the loaded 3D GMOT shows the highest atom number reported so far in a grating based system, likely due to the improved vacuum quality of the 3D GMOT chamber.

These results encourage further development and integration of gratings into future cold atom experiments. In particular, gratings are easily integrated into atom chip designs, in which magnetic fields are created with currents on microchips instead of large coil-based systems. GMOT's specifically aid alignment of atomic clouds with small chip features, further suggesting their use in field-deployable devices.

## VII. ACKNOWLEDGEMENTS

We would like to thank the Air Force Office of Scientific Research for its support of this work, as well as the

Department of Energy's Center for Integrated Nanotechnologies for its expertise in lithographic techniques and grating manufacture. We appreciate the research group of Erling Riis at the University of Strathclyde and their expertise in GMOT design.

- 
- [1] B. Barrett, I. Chan, and A. Kumarakrishnan, *Physical Review A* **84** (2011).
  - [2] S. B. Cahn, A. Kumarakrishnan, U. Shim, T. Sleator, P. R. Berman, and B. Dubetsky, *Physical Review Letters* **79** (1997).
  - [3] A. Cronin, J. Schmiedmayer, D. Pritchard, *Reviews of Modern Physics* **81** (2009).
  - [4] C. Adams, M. Sigel, J. Mlynek, *Physics Reports* **240** (1993).
  - [5] D. Durfee, Y. Shaham, M. Kasevich, *Physical Review Letters* **97** (2006).
  - [6] S.M. Dickerson, J.M. Hogan, A. Sugarbaker, D.M.S. Johnson, and M.A. Kasevich, *Physical Review Letters* **111** (2013).
  - [7] J. E. Debs, N. P. Robins, and J. D. Close, *Science* **339** (2013).
  - [8] T. Kovachy, P. Asenbaum, C. Overstreet, C. A. Donnelly, S. M. Dickerson, A. Sugarbaker, J. M. Hogan, and M. A. Kasevich, *Nature* **528** (2015).
  - [9] J. M. Hogan, D. M. S. Johnson, S. Dickerson, T. Kovachy, A. Sugarbaker, S. Chiow, P. W. Graham, M. A. Kasevich, B. Saif, S. Rajendran, P. Bouyer, B. D. Seery, L. Feinberg, R. Keski-Kuha, *General Relativity and Gravitation* **43** (2011).
  - [10] E. Imhof, J. Stickney, and M. Squires, *Atoms* **4** (2016).
  - [11] H. Muntinga, et al., *Physical Review Letters* **110** (2013).
  - [12] J. A. Rushton, M. Aldous, and M. D. Himsforth, *Review of Scientific Instruments* **85** (2016).
  - [13] J. Williams, S. Chiow, N. Yu, H. Muller, *New Journal of Physics* **18** (2016).
  - [14] B. Barrett, L. Antoni-Micollier, L. Chrichet, B. Battelier, T. Leveque, A. Landragin, and P. Bouyer, *Nature Communications* **7** (2016).
  - [15] R. Geiger, V. Menoret, G. Stern, N. Zahzam, P. Cheinet, B. Battelier, A. Villing, F. Moron, M. Lours, Y. Bidel, A. Bresson, A. Landragin, and P. Bouyer, *Nature Communications* **2** (2011).
  - [16] K. S. Hardman, P. J. Everitt, G. D. McDonald, P. Manju, P. B. Wigley, M. A. Sooriyabandara, C. C. N. Kuhn, J. E. Debs, J. D. Close, and N. P. Robins, *Physical Review Letters* **117** (2016).
  - [17] M. Keil, O. Amit, S. Zhou, D. Groswasser, Y. Japha, and R. Folman, *Journal of Modern Optics* **63** (2016).
  - [18] C.C. Nshii, et. al., *Nature Nanotechnology* **8**, 321 (2013).
  - [19] M. Vangeleyn, P. F. Griffin, E. Riis, A.S. Arnold, *Optics Letters* **35** (2010).
  - [20] J. Esteve, *Nature Nanotechnology* **8** (2013).
  - [21] J. Lee, J. A. Grover, L.A. Orozco, and S. L. Rolston, *Journal of the Optical Society of America B* **30** (2013).
  - [22] K. Dieckmann, R. J. C. Spreeuw, M. Weidemuller, and J. T. M. Walraven, *Physical Review A* **58** (1998).
  - [23] M. Vangeleyn, *Atom trapping in non-trivial geometries for micro-fabrication applications*, Ph.D. thesis, University of Strathclyde (2011).
  - [24] J. P. McGilligan, P. F. Griffin, E. Riis, and A.S. Arnold, *Optics Express* **23** (2015).
  - [25] J. P. McGilligan, P. F. Griffin, E. Riis, and A.S. Arnold, *Journal of the Optical Society of America B* **33** (2016).
  - [26] J.P. Cotter, J.P. McGilligan, P.F. Griffin, I.M. Rabey, K. Docherty, E. Riis, A.S. Arnold, and E.A. Hinds, *Applied Physics B* **122** (2016).
  - [27] M. B. Squires, S. E. Olson, B. Kasch, J. A. Stickney, C. J. Erickson, J. A. R. Crow, J. E. Carlson, and J. H. Burke, *Applied Physics Letters* **109** (2016).
  - [28] K. Dieckmann, et. al., *Physical Review A* **58** (1998).
  - [29] J. Schoser, et. al., *Physical Review A* **66** (2002).
  - [30] J. Ramirez-Serrano, et. al., *Optics Letters* **31** (2006).
  - [31] J. Kellogg, et. al., *Applied Physics B* **109**, 61 (2012).

## Appendix A: 2D GMOT Derivation

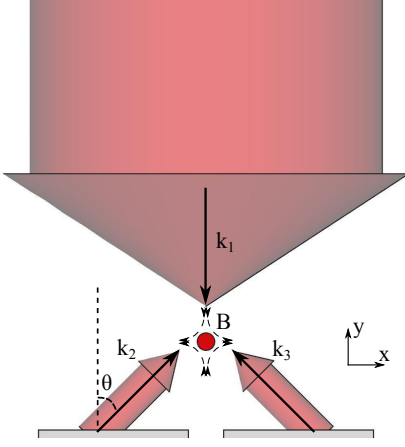


FIG. 10. (Color online) The  $\mathbf{k}$  vectors and  $\mathbf{B}$  field to model a 2D GMOT.

The average force from the  $j^{th}$  beam is

$$\mathbf{F}_j \approx \hbar \mathbf{k}_j \frac{\Gamma}{2} \frac{I_j}{I_{sat}} \left[ K + C \left( \mathbf{k}_j \cdot \mathbf{v} - \frac{\mu_F s}{\hbar} \frac{\mathbf{k}_j \cdot \mathbf{B}}{|\mathbf{k}_j|} \right) \right]. \quad (\text{A1})$$

The magnetic field is  $\mathbf{B} = G\langle x, -y \rangle$ . The three beams have  $\mathbf{k}$  vectors,

$$\mathbf{k}_1 = k\langle 0, -1 \rangle$$

with polarization  $s = +1$  and

$$\mathbf{k}_2 = k\langle \sin \theta, \cos \theta \rangle$$

$$\mathbf{k}_3 = k\langle -\sin \theta, \cos \theta \rangle$$

with fraction  $P_+$  in the  $s = +1$  polarization and the remainder  $P_-$  in the  $s = -1$  polarization, where  $\theta$  is the diffraction angle from the  $+\hat{\mathbf{y}}$  axis.

### 1. Beam 1

For the input beam,

$$\begin{aligned} \mathbf{F} &\approx \hbar \mathbf{k}_1 \frac{\Gamma}{2} \frac{I_1}{I_{sat}} \left[ K + C \left( \mathbf{k}_1 \cdot \mathbf{v} - \frac{\mu_F s}{\hbar} \frac{\mathbf{k}_1 \cdot \mathbf{B}}{|\mathbf{k}_1|} \right) \right] \\ &\approx -\hbar k \frac{\Gamma}{2} \frac{I_1}{I_{sat}} \left[ K + C \left( -kv_y - \frac{\mu_F G}{\hbar} y \right) \right] \hat{\mathbf{y}}. \end{aligned} \quad (\text{A2})$$

### 2. Beam 2

For the  $s = +1$  fraction of the second beam,

$$\begin{aligned} \mathbf{F} &\approx \hbar k \langle \sin \theta, \cos \theta \rangle \frac{\Gamma}{2} \frac{P_+ I_2}{I_{sat}} \left[ K + C \left( kv_x \sin \theta \right. \right. \\ &\quad \left. \left. + kv_y \cos \theta - \frac{\mu_F G}{\hbar} x \sin \theta + \frac{\mu_F G}{\hbar} y \cos \theta \right) \right]. \end{aligned} \quad (\text{A3})$$

For the  $s = -1$  fraction of the second beam,

$$\begin{aligned} \mathbf{F} &\approx \hbar k \langle \sin \theta, \cos \theta \rangle \frac{\Gamma}{2} \frac{P_- I_2}{I_{sat}} \left[ K + C \left( kv_x \sin \theta \right. \right. \\ &\quad \left. \left. + kv_y \cos \theta + \frac{\mu_F G}{\hbar} x \sin \theta - \frac{\mu_F G}{\hbar} y \cos \theta \right) \right]. \end{aligned} \quad (\text{A4})$$

### 3. Beam 3

For the  $s = +1$  fraction of the third beam,

$$\begin{aligned} \mathbf{F} &\approx \hbar k \langle -\sin \theta, \cos \theta \rangle \frac{\Gamma}{2} \frac{P_+ I_3}{I_{sat}} \left[ K + C \left( -kv_x \sin \theta \right. \right. \\ &\quad \left. \left. + kv_y \cos \theta + \frac{\mu_F G}{\hbar} x \sin \theta + \frac{\mu_F G}{\hbar} y \cos \theta \right) \right]. \end{aligned} \quad (\text{A5})$$

For the  $s = -1$  fraction of the third beam,

$$\begin{aligned} \mathbf{F} &\approx \hbar k \langle -\sin \theta, \cos \theta \rangle \frac{\Gamma}{2} \frac{P_- I_3}{I_{sat}} \left[ K + C \left( -kv_x \sin \theta \right. \right. \\ &\quad \left. \left. + kv_y \cos \theta - \frac{\mu_F G}{\hbar} x \sin \theta - \frac{\mu_F G}{\hbar} y \cos \theta \right) \right]. \end{aligned} \quad (\text{A6})$$

### 4. Total Forces

Combining the contributions of each beam in the  $\hat{\mathbf{x}}$  direction with  $I_{up} = I_1 = I_2$  and  $P_+ + P_- = 1$ ,

$$\mathbf{F}_{tot,x} \approx \hbar k C \Gamma \sin^2 \theta \frac{I_{up}}{I_{sat}} \left( kv_x + (P_- - P_+) \frac{\mu_F G}{\hbar} x \right). \quad (\text{A7})$$

Similarly,

$$\begin{aligned} \mathbf{F}_{tot,y} &\approx \hbar k \cos \theta \frac{\Gamma}{2} \frac{I_{up}}{I_{sat}} \left( 2K + \left[ 2C \left( kv_y \cos \theta \right. \right. \right. \\ &\quad \left. \left. + 2(P_+ - P_-) \frac{\mu_F G}{\hbar} y \cos \theta \right) \right] \right) \\ &\quad - \hbar k \frac{\Gamma}{2} \frac{I_1}{I_{sat}} \left[ K + C \left( -kv_y - \frac{\mu_F G}{\hbar} y \right) \right]. \end{aligned} \quad (\text{A8})$$

For the constant terms (i.e. those  $\propto K$ ) to cancel,  $I_{up} = I_1/2 \cos \theta$ . Then,

$$\mathbf{F}_{tot,y} \approx \hbar k C \frac{\Gamma}{2} \frac{I_1}{I_{sat}} \left( kv_y (1 + \cos \theta) + \frac{\mu_F G}{\hbar} y (1 + (P_+ - P_-) \cos \theta) \right). \quad (\text{A9})$$



## Appendix B: GMOT Distribution Derivation

### 1. Beam Distribution

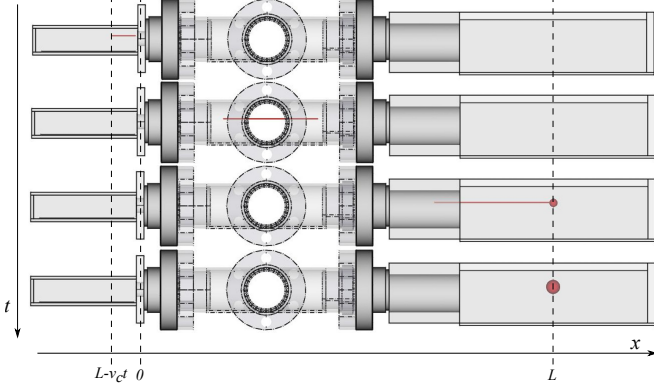


FIG. 11. (Color online) A short pulse of the 2D<sup>+</sup> GMOT is released at  $t = 0$ , traverses a distance  $L$ , and is captured in a 3D GMOT, which grows as a function of time.

When the plug beam is pulsed off for a short period, a small packet of atoms from the 2D<sup>+</sup> GMOT is allowed to pass through the pinhole, across a distance  $L$ , to the 3D GMOT trapping region. If the atoms from the beam packet are slower than the capture velocity  $v_c$ , they will be collected into the 3D GMOT, which will grow with increased atom number. The process is illustrated in Fig. 11.

Define the pinhole to be at  $x = 0$ . Assume that at  $t = 0$ , the atoms are distributed uniformly behind the pinhole ( $x < 0$ ) with no atoms past the pinhole ( $x > 0$ ). Assume the atoms have a Gaussian distribution in velocity. The number of atoms between  $x$  and  $x + dx$  with velocities between  $v$  and  $v + dv$  is given by

$$\eta(x, v) dx dv = \frac{A}{\sigma\sqrt{2\pi}} \exp\left(-\frac{(v - v_0)^2}{2\sigma^2}\right) dx dv \quad (\text{B1})$$

where  $v_0$  is the peak velocity of the distribution and  $\sigma$  is the velocity spread.  $A$  represents the number of atoms/m, which is weighted by a normal distribution in velocity. The total number of atoms with initial positions between  $x_1$  and  $x_2$  with velocities between  $v_1$  and  $v_2$  is

$$N = \int_{x_2}^{x_1} \int_{v_1}^{v_2} \eta(x, v) dv dx \quad (\text{B2})$$

The 3D GMOT size at time  $t$  is proportional to the number of atoms that reach the point  $x = L$  with velocities less than  $v_c$  at or before time  $t$ . In other words, an atom at position  $x$  must travel at least  $L + |x|$  in time  $t$ . Accordingly, the minimum velocity that reaches the 3D GMOT by time  $t$  is  $v_1 = (L + |x|)/t$ . The velocity range that can effect the 3D GMOT at time  $t$  is then  $[v_1, v_2] = [(L - x)/t, v_c]$ .

At  $t = 0$ , no atoms exist past the pinhole, so  $x_2 = 0$ . The fastest atom capable of being trapped is  $v_c$ , and it

can only travel a distance  $v_c t$  in time  $t$ . The fastest atom can have an initial position no further behind the pinhole than  $x_1 = L - v_c t$ . Using these limits, the total number of atoms that reach the 3D GMOT by time  $t$  is

$$\begin{aligned} N(t) &= \int_{L-v_c t}^0 \int_{(L-x)/t}^{v_c} \eta(x, v) dv dx \\ &= \frac{A}{\sigma\sqrt{2\pi}} \int_{L-v_c t}^0 \int_{(L-x)/t}^{v_c} \exp\left(-\frac{(v - v_0)^2}{2\sigma^2}\right) dv dx \\ &= \frac{A}{2} \int_{L-v_c t}^0 \operatorname{erf}\left[\frac{v_0 - \frac{L-x}{t}}{\sigma\sqrt{2}}\right] dx - \frac{A}{2} \int_{L-v_c t}^0 \operatorname{erf}\left[\frac{v_0 - v_c}{\sigma\sqrt{2}}\right] dx. \\ &= A \frac{\sigma t}{\sqrt{2\pi}} \left( \exp\left[-\frac{(\frac{L}{t} - v_0)^2}{2\sigma^2}\right] - \exp\left[-\frac{(v_0 - v_c)^2}{2\sigma^2}\right] \right) \\ &\quad + \frac{A}{2} (v_0 t - L) \operatorname{erf}\left[\frac{v_0 - \frac{L}{t}}{\sigma\sqrt{2}}\right] - \frac{A}{2} t (v_0 - v_c) \operatorname{erf}\left[\frac{v_0 - v_c}{\sigma\sqrt{2}}\right] \\ &\quad + \frac{A}{2} (L - v_c t) \operatorname{erf}\left[\frac{v_0 - v_c}{\sigma\sqrt{2}}\right]. \end{aligned} \quad (\text{B3})$$

### 2. Flux Distribution

Define the total flux, in atoms/second at speeds between  $v_1$  and  $v_2$ , as  $\int_{v_1}^{v_2} \Phi(v) dv$ .  $\Phi(v)$  can be derived knowing  $\eta(x, v)$ . The number of atoms at speed  $v'$  in the 2D<sup>+</sup> GMOT distribution that exit the pinhole in time  $t$  is given by

$$\begin{aligned} N(v', t) &= \int_{-v' t}^0 \int_{v'}^{v' + dv} \eta(x, v) dv dx \\ &= \int_{-v' t}^0 [\eta(x, v') dv] dx \\ &= A \int_{-v' t}^0 \left[ \frac{1}{\sigma\sqrt{2\pi}} \exp\left(-\frac{(v' - v_0)^2}{2\sigma^2}\right) \right] dx \\ &= \frac{Av' t}{\sigma\sqrt{2\pi}} \exp\left(-\frac{(v' - v_0)^2}{2\sigma^2}\right) dv. \end{aligned} \quad (\text{B4})$$

Thus, the flux of atoms in a narrow range of velocities between  $v$  and  $v + dv$  is

$$\Phi(v) dv = \frac{N(v, t)}{t} = \frac{A}{\sigma\sqrt{2\pi}} v \exp\left(-\frac{(v - v_0)^2}{2\sigma^2}\right) dv. \quad (\text{B5})$$

Which peaks when  $v = (v_0 \pm \sqrt{v_0^2 + 4\sigma^2})/2$ . The total flux that was blocked by the plug beam is

$$\int_{-\infty}^{\infty} \Phi(v) dv = Av_0. \quad (\text{B6})$$